On how mild oxidation affects the structure of carbons: Comparative analysis by different techniques

Gianluca Levi [a,1], Mauro Causà [a,b], Luciano Cortese [b], Piero Salatino [b], Osvalda Senneca [b,*]

[a] *Dipartimento di Ingegneria Chimica, dei Materiali e della Produzione Industriale, Università degli Studi di Napoli, Italy*
[b] *Istituto di Scienze e Tecnologie per l'Energia e la Mobilità Sostenibili, Consiglio Nazionale delle Ricerche, Napoli, Italy*

A R T I C L E   I N F O

A B S T R A C T

Understanding how the structure of carbonaceous materials changes upon oxidation at mild temperature as a function of the graphitic order is of great importance for the development of clean combustion technologies, such as carbon fuel cells. The micro- and nanostructures of a range of carbon materials at room temperature and upon mild oxidation at 300 °C have been analysed by means of mercury porosimetry, Nitrogen adsorption, X-Ray Diffraction, Raman spectroscopy and Electron Paramagnetic Resonance. The samples included carbons with increasing level of graphitic order: three chars derived from two bituminous coals and a lignite, a synthetic carbon and a graphitized coke. The experimental characterization allows to classify the materials according to different structural parameters, including porosity, surface area, degree of graphitization and paramagnetic activation of the carbonaceous surface. A correlation with the rank of the analysed materials is observed. For the graphitized coke, oxidation leads to more crystalline order and enhancement of the paramagnetic signal. A similar increase in the paramagnetic activity is observed for the Lignite char. On the other hand, for the higher rank, bituminous and synthetic chars, mild oxidation leads to a slight expansion of the amorphous carbon and loss of paramagnetic activity. The differences are rationalized in terms of formation of new carbon-oxygen complexes on the graphitized coke and on the Lignite char, and redistribution of already existing complexes for the higher-rank coals. This investigation complements previous X-ray photoelectron spectroscopy measurements.

Introduction

As a carbon material comes into contact with O_2 in air, uptake of O_2 and change in the carbonaceous molecular [1] and supramolecular [2] structures occur. Most of the studies that address the nature and extent of microstructural changes of coals and coal chars upon oxidation are performed at temperatures typical of combustion (> 400 °C) [3–6]. Fewer recent studies investigate the oxidation of carbons at mild temperatures (below 300 °C). Most of them focus on the conditions that lead to the spontaneous ignition of coal [7–12]. For example, Xiao et al. [10] have analyzed the structure of coal upon oxidation at 140–350 °C by Fourier-transform infrared spectroscopy and X-Ray Diffraction (XRD). These authors observed that the stacking height of the carbon domains increases together with the content of aliphatic and aromatic hydrocarbons, and oxygen-containing functional groups. Recently, mild oxidation of carbons has also raised particular interest because it can be exploited in applications such as ion batteries, supercapacitors and innovative clean combustion technologies, such as carbon fuel cells [13–16]. In the case of pitch, for instance, it has been shown that the

introduction of oxygen-based functional groups is the key to achieve a highly disordered structure, ensuring the appropriate cross-linkage and limiting melting and rearrangement of the carbon structure upon high-temperature carbonization [17]. The carbon materials used in applications for clean energy production include both disordered carbon materials, such as coal or biogenic carbons, and more ordered carbons, such as chars, coke and graphene. The efficiency of energy conversion depends on the microstructure and functionality of the carbon material and how they change upon mild oxidation as a function of the degree of graphitic order. Therefore, characterizing the effect of mild oxidation across a broad range of carbon structures is essential, but such studies are currently lacking. A comprehensive study on mild oxidation of carbons using a multitude of experimental techniques has never been carried out for the temperature of oxidation of 200–300 °C.

In a recent work, a selection of coal chars obtained from coals of different rank and a synthetic carbon (Carboxen) has been characterised after oxidation in air at moderate temperatures by X-ray photoelectron spectroscopy (XPS) [1]. Deconvolution of the O 1s spectra provided clues on epoxidation as being the prevalent type of oxygen function-

---

Table 1
Proximate and ultimate analysis of carbon samples.

	Graphitized Coke	Lignite char	South African char	Colombian char	Carboxen
Proximate analysis (w%)					
Residual volatile matter	1.9	15.8	4.6	7.5	5.0
Fixed carbon	89.1	46.7	75.0	84.9	92.0
Ash	9.0	37.5	20.4	7.6	3.0
Ultimate analysis (w%)					
Carbon	90.3	53.8	75.4	83.9	92.0
Hydrogen	0.3	1.2	1.2	1.1	0.7
Nitrogen	0.4	1.3	1.8	1.8	0.1

alization at room temperature for all the investigated carbons [1,18]. Moreover, a pronounced loss of C sp^2 hybridization after oxidation in air at 300 °C (200 °C for a Lignite char) was deduced from the evolution of the C 1s and valence band spectra. The present study complements our previous investigation [1] by applying an extensive array of experimental techniques to characterize the microstructure of different carbon materials, namely: porosimetric analysis; Raman spectroscopy, Electron Paramagnetic Resonance (EPR) spectroscopy, XRD. The scope is to characterize these materials according to the degree of crystalline order and porosity and to assess whether there are differences in the changes of the structure and paramagnetic activity upon mild oxidation.

By characterizing the effects of oxidation on the structure of carbon materials with different degrees of graphitic order at temperatures typical of the operating conditions of clean combustion processes, the present study will help promote the further development of innovative combustion techniques.

Experimental

Materials

The present study has been carried out on five different solid carbon samples: a polycrystalline graphitic material (coke) and four turbostratic carbons. The turbostratic samples comprise a synthetic carbon and three chars obtained from coals of different rank and origin. The synthetic carbon was supplied by Sigma-Aldrich under the name of "Carboxen 1000" (further called "Carboxen", it is also known as "Spherocarb"). It is a spherically shaped 60/80-mesh carbon commonly used as molecular sieve in gas chromatography. It is synthesized by pyrolysis of an organic polymeric precursor and has been used in prior studies to model the behaviour of char under oxidative conditions [19]. The three chars were obtained from a Lignite from Montana, which is a young, low-rank coal with a relatively high content of volatiles, and two bituminous, medium-rank coals, a South African and a Colombian coal. To obtain the chars the coals were pyrolyzed in a lab-scale fluidized bed reactor at 850 °C in N$_2$ flow for 5 min, a time long enough to release most volatile matter and convert the amorphous carbon into turbostratic carbon. The residual char particles were ground and sieved to the size of 100–150 μm and stored in sealed vials under moderate vacuum. This procedure avoids uncontrolled oxidation and uptake of moisture from atmospheric air. The properties of the different samples are reported in Table 1. The graphitic material is characterized by a high carbon content and limited content of volatile matter.

Oxidation treatment

The samples were subjected to mild oxidation treatments according to the following procedure. After grinding, the samples were placed in a cylindrical stainless steel reactor and continuously flushed with air while heating up to 300 °C by an external oven. Eventually, they were held at the final temperature for a time ranging between 2 to 10 h. Since Lignite char is known to be very reactive towards oxidation, for this sample the temperature of oxidation was limited to 200 °C, which prevents extensive combustion. As for the original samples, oxidized samples were

stored in sealed vials under moderate vacuum prior to further analysis. The samples, subjected to the same oxidation treatment, have also been characterized by means of high-resolution XPS spectroscopy in a previous work [1].

Porosimetric analysis

Nitrogen adsorption measurements were carried out in a Quantachrome Autosorb 1 C area and porosity analyser. The samples (about 0.20 g each) were degassed under vacuum (10 μm Hg) at 150 °C for times between 4–12 h on the degassing port of the equipment prior to adsorption (77 K in liquid N$_2$). The adsorption data were automatically acquired, and data in the relative pressure range 0 < P/Po ⩽ 0.30 used for BET (Brunauer–Emmett–Teller) analysis. For N$_2$ adsorption on coals, P/Po is usually limited to ~0.3 as this relative pressure range corresponds to a multi-layer coverage of few layers of N$_2$. At higher P/Po values, condensation of N$_2$ in the pores occurs, leading to a large error and a significantly lower predicted surface area.

Mercury Intrusion Porosimetry (MIP) measurements were obtained using a Micromeritics AutoPore IV 9500 instrument. The samples were first degassed at the low-pressure port (<50 μm Hg). After evacuation, the samples were pressurized in the high-pressure port where mercury intrusion takes place. Both degassing and intrusion are controlled automatically. Samples can be pressurized from 1.5 to 60000 psi. The mercury contact angle and surface tension during intrusion were assumed to be 130° and 0.485 Nm^{-1}, respectively. Due to the small particle size (100 μm) problems arise at low pressure with the inter-particle voids. Data have been worked out to evaluate the volume and the size distribution (dV/dlog(r)) of pores with diameter smaller than 1000 nm, which corresponds to values of pressure above 15 psi. The reproducibility of the results was checked by repeated tests.

X-ray diffraction analysis

The XRD profiles of the raw and oxidized samples were recorded using a Bruker D2 Phaser apparatus with Cu Kα radiation (30 kV, 10 mA) as X-ray source. Scattered X-ray intensities were collected over a range of scattering angle 2θ = 5-75° with a scan velocity of 0.05 2θs^{-1}. The percentage of amorphous vs. crystalline matter was computed using Bruker's software DIFFRAC-EVA after subtraction of the background signal. When the (002) band centered at about 2θ = 25° was found to be asymmetric, this was attributed to superposition of another peak, the γ band, at lower 2θ values [20,21]. In these cases, a decomposition by non-linear curve fitting of the spectra was carried out, where the γ and (002) band were fitted using Gaussian functions [22]. The fraction of aromatic vs. aliphatic carbon in the crystalline matter was then calculated from the ratio of the areas under the two deconvoluted γ and (002) bands. The mean interlayer spacing d_{002} of the graphitic or turbostratic crystallites was calculated by applying Bragg's law using the (002) band after background subtraction and deconvolution. The average stacking height (L_a) and average diameter (L_a) of the graphene layers were calculated using Scherrer formulas. From the values of d_{002} and L_c, the number of layers per crystallite n_A, was calculated as: $n_A = L_c/d_{002} + 1$.

The fraction f_a of aromatic vs aliphatic carbon was calculated from the ratio of the areas under the γ and (002) bands according to

$$f_a = \frac{C_A}{C_A + C_S} = \frac{A_{002}}{A_{002} + A_\gamma}$$

where A represents the integrated area of the peak, while C_A and C_S are the number of aromatic and aliphatic (saturated) carbon atoms per structural unit, respectively.

Raman measurements

Raman spectra were recorded with an XploRA micro-Raman spectrometer operated in a backscattered configuration. The spectrometer was equipped with an Olympus BX41 100 × microscope and a Nd:Yag laser source (λ_0 = 514 nm, source power 14 mW). Raman spectra were recorded between 950 and 2200 cm^{-1}. The area measured by the focused Nd:Yag laser beam was a few μm^2. The power of the laser beam was set at 10% (1.4 mW). Spectra acquisition for each sample was performed at different locations to test reproducibility. A nonlinear baseline was subtracted to get rid of the fluorescence background and curve fitting was performed with the software Origin (OriginLab, Levenberg–Marquardt fitting algorithm [23]). The spectra were fitted with a combination of three bands: the D, 'Defective' (Lorentzian), G, 'Graphitic' (Lorentzian), and D3 (Gaussian) bands, centred at around 1340, 1595 and 1500 cm^{-1}, respectively. No D3 band was found in the spectra of the graphitized coke; however, an additional D2 Lorentzian band at ~1620 cm^{-1} was found to be needed in the fitting in this case. This band arises from a double resonant process activated by defects, such as edge defects, that break the symmetry of the graphene planes [24]. The spectra were normalized with respect to the G band at ~1580 cm^{-1}, which was found to be the most intense band in all cases. From the values of the ratio I_D/I_G, where I is the peak area, the average diameter (L_a) of the graphene layers was evaluated using the Tuinstra and Koenig relation [25] with C(514 nm) = 4.4 nm. The relative content of amorphous sp^2 carbon was estimated from the ratio I_{D3}/I_G [26].

Electron paramagnetic resonance measurements

The EPR spectra were measured using an X-band (9.351 GHz) EPR spectrometer. Each spectrum was obtained by monitoring the microwave absorption as the magnetic field is changed between 500 and 5500 G. The EPR signal was recorded as the first derivative of the absorption. The resonance condition is normally written as:

$$h\upsilon = g\beta B$$

where h is the Planck constant (6.62608 × 10^{-34} Js), υ is the frequency of the microwave source (9.351 GHz), β is the Bohr magneton (9.2740 × 10^{-24} JT^{-1}) and B is the magnetic field at resonance. Bands were assigned based on their g values according to the classification system proposed by Ottaviani et al. [27–28]. The peak-to-peak amplitude (A_{pp}) and peak-to-peak width (ΔB_{pp}) were obtained as illustrated in Fig. 1.

Results

Porosimetric analysis

Fig. 2 reports the N_2 adsorption and desorption isotherms obtained for the different samples before and after oxidation. Additional figures which better show the shape of the curves in the low P/Po region are reported in Supplementary Material. BET areas obtained from N_2 adsorption are reported in Table 2.

Inspection of the nitrogen adsorption/desorption curves reveals that the Carboxen stems out of the group, being the only sample with a marked convexity in the P/Po range 0-0.8. In fact, the Carboxen is the only sample with extensive microporosity and high value of BET
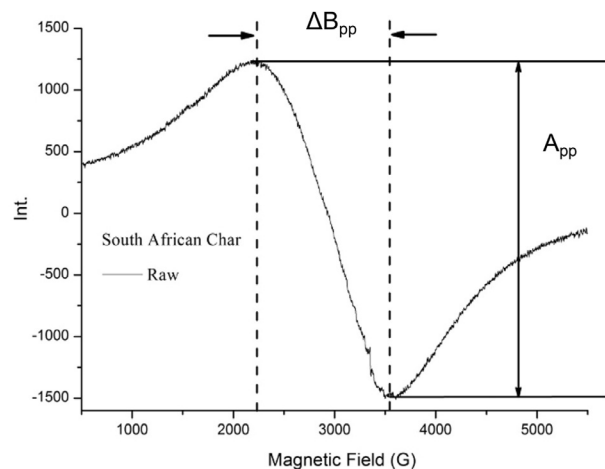
Fig. 1. Schematic illustration of how the parameters A_{pp} and ΔB_{pp} are obtained from the EPR spectra.

area (744 m^2/g), which is an order of magnitude bigger than for the other samples. Analysis of the Nitrogen adsorption curve according to the Barrett-Joyner-Halenda (BJH) [29] method shows a bimodal pore size distribution with a smaller fraction of pores with d_p = 3 nm and a larger fraction of pores with d_p = 50 nm (the pore size distribution is reported in Supplementary Material).

In the Lignite char and coke the shape of the adsorption isotherms indicates that both micro- and mesoporosity are negligible. The steep increase close to saturation pressure indicates filling of larger pores. An H3 type hysteresis according to IUPAC classification is observed, which is common in non-rigid aggregates of plate-like particles and slit-shaped pores. Forced closure of the hysteresis loop due to the so-called tensile effect is also observed. The Colombian and South African chars in the low pressure range display a slope consistent with negligible microporosity and H3 hysteresis, however some porosity is disclosed in the meso-macropore range. The BET areas are respectively 34 and 18 m^2/g and the average pore diameters are 900 and 500 nm. The population of pores in the South African char appears more uniform compared to the pore size distribution of the other coal chars.

Fig. 3 reports the mercury intrusion curves of the different samples before and after oxidation in the investigated pressure range. It can be observed that a large volume of mercury was intruded at low pressure in all samples (corresponding to large pore diameters). This phenomenon is an artefact related to the interparticle voids and depends on the particle size distribution of the sample. For instance, in the Carboxen, which has a rather regular spherical shape of nominal size of 60–80 mesh (d = 200 μm), interparticle voids of 20–30 μm diameter are observed. In the other samples, the size distribution of interparticle voids is wider due to the less regular shape and particle size distribution. In these cases, it is difficult to draw a clear distinction between internal porosity and interparticle voids. Based on the inspection of the curves, an upper cut-off to the pore size range was set at 1 μm. The pore volume and average pore diameter for this pore size range are reported in Table 2.

Analysis of the mercury intrusion curves confirm that Carboxen is the most porous of the samples investigated, having a very large fraction of pores of diameter d_p in the order of 50 nm. The specific pore volume measured by mercury intrusion is much smaller for all other samples and decreases in the order: Lignite>oke>Colombian>South African. The modest porosity of coal chars should not surprise since, as reported in previous studies [30], soon after devolatilization the pore network of chars is often "locked" (possibly by recondensation of volatile matter at the pore entrance) and becomes accessible only after some degree of combustion, when amorphous matter obstructing the pore entrances is consumed.
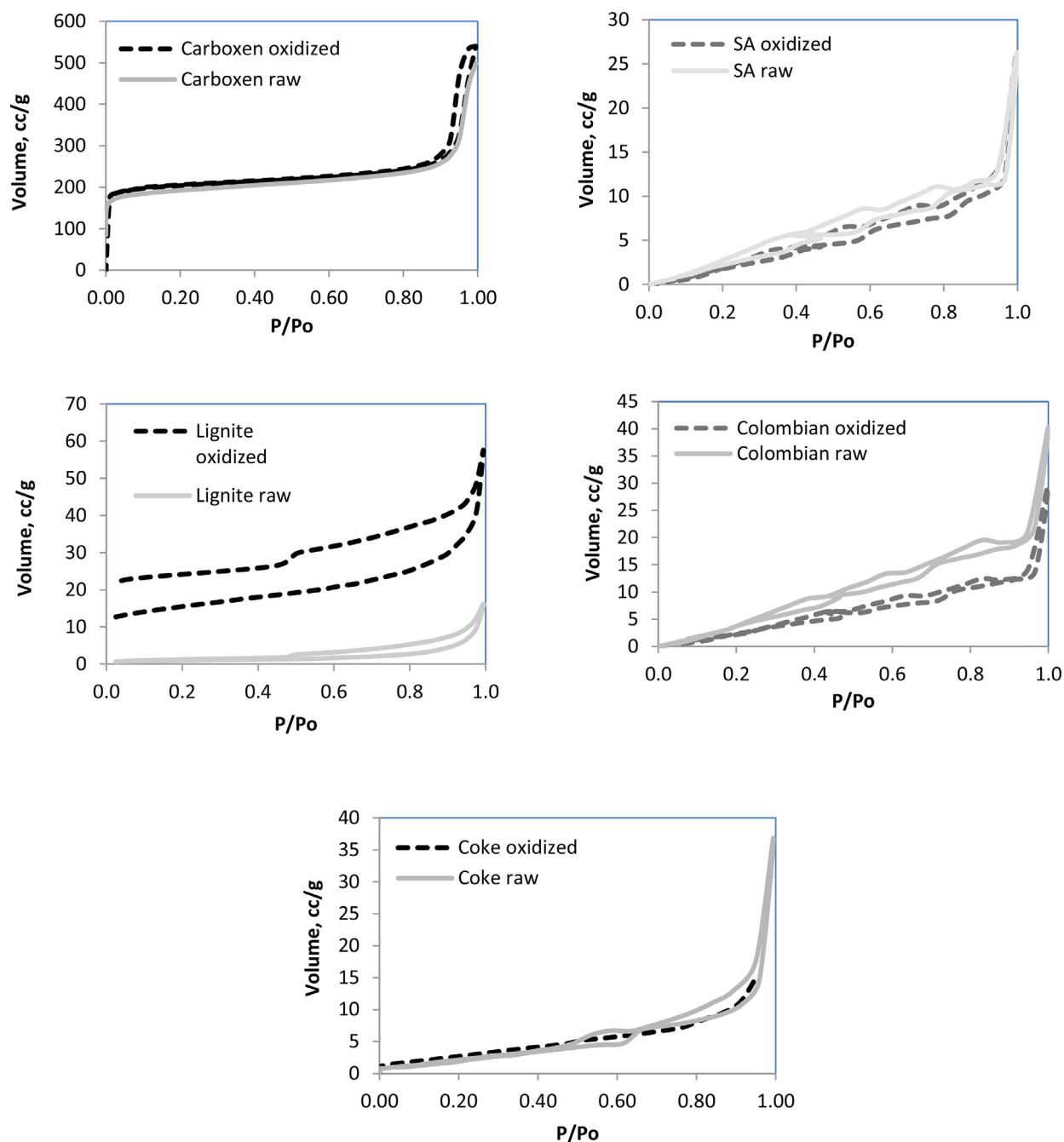
Fig. 2. N$_2$ adsorption-desorption isotherms before and after oxidation. SA =South African.

Table 2
Results of the porosimetric analysis.

Sample	Oxidation	N2 77K	Mercury porosimetry		
		BET area m^2/g	Volume mm^3/g (d_p < 1 µm)	Volume mm^3/g (d_p < 3.5 µm)	Pore radius
nm					
Lignite char	Raw	8	140	170	42.00
	200 °C 3 h	53	146	193	52.00
South African char	Raw	18	100	230	255.00
	300 °C 2 h	17	41	97	607.00
Colombian char	Raw	34	175	364	452.00
	300 °C 2 h	21	130	400	580.00
Carboxen	Raw	744	496	496	25.00
	300 °C 2 h	866	560	614	31.00
Graphitized coke	Raw	11	126	200	94.00
	300 °C 3 h	12	120	197	217.00
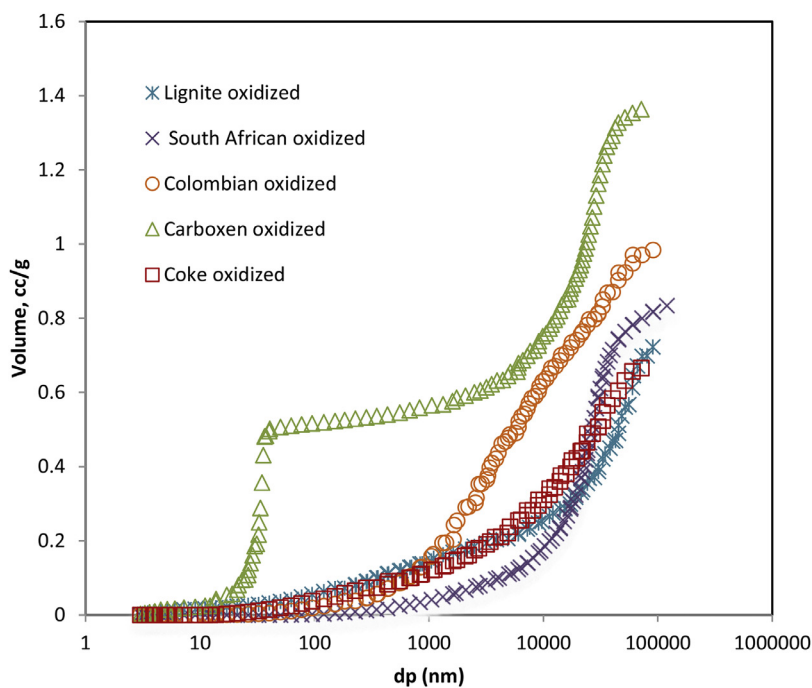
Fig. 3. Mercury intrusion curves before (bottom) and after (top) oxidation.
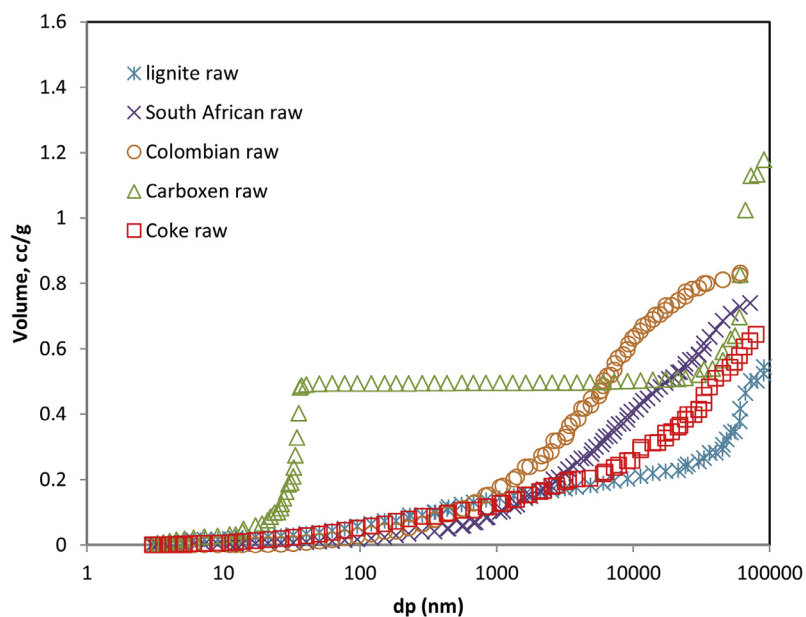
Upon oxidation, the Lignite char exhibits the most significant changes in terms of nitrogen adsorption, with a vertical shift of the N_2 adsorption isotherm and a clear increase of BET area. On the contrary, mercury intrusion curves do not show any relevant changes up to 1 μm upon oxidation. Moreover, we note that the isotherm of the oxidized Lignite char exhibits a singular behaviour in the desorption stage, with a pronounced hysteresis which fails to close. This type of phenomenon is in general ascribed to changes in volume of the adsorbent (swelling) or irreversible uptake of molecules. In the Carboxen, oxidation leads to a slight increase of porosity, both in terms of nitrogen adsorption and of mercury intrusion. On the contrary, in the Colombian and South African chars the effect of oxidation is to reduce the BET area as well as the volume of intruded mercury. In the graphitized coke the pore volume measured by MIP also decreases upon oxidation but the BET area remains relatively constant.

In order to explain the observed behavior we shall firstly consider the differences in combustion reactivity among the examined carbonaceous samples. At one extreme, there is coke, which amongst the examined samples is the least reactive, due to its relatively high degree of graphitization and low mineral matter content: carbon consumption for coke under mild oxidative conditions is indeed negligible, therefore changes in porosity and surface area are irrelevant. At the other extreme, there is Lignite, which is the most reactive material due to its low coalification degree and also to the high content of mineral matter, which in lignites is typically constituted by disperse and catalytically active metals (such as Ca, Na, K, Fe, Mg): The experimental oxidation conditions are in this case sufficient to produce a non negligible extent of carbon consumption and, in particular, to remove the amorphous carbon matter which blocks small pores, thus increasing BET surface areas. The reactivity of the Carboxen and the coal chars stands in between that of Lignite and
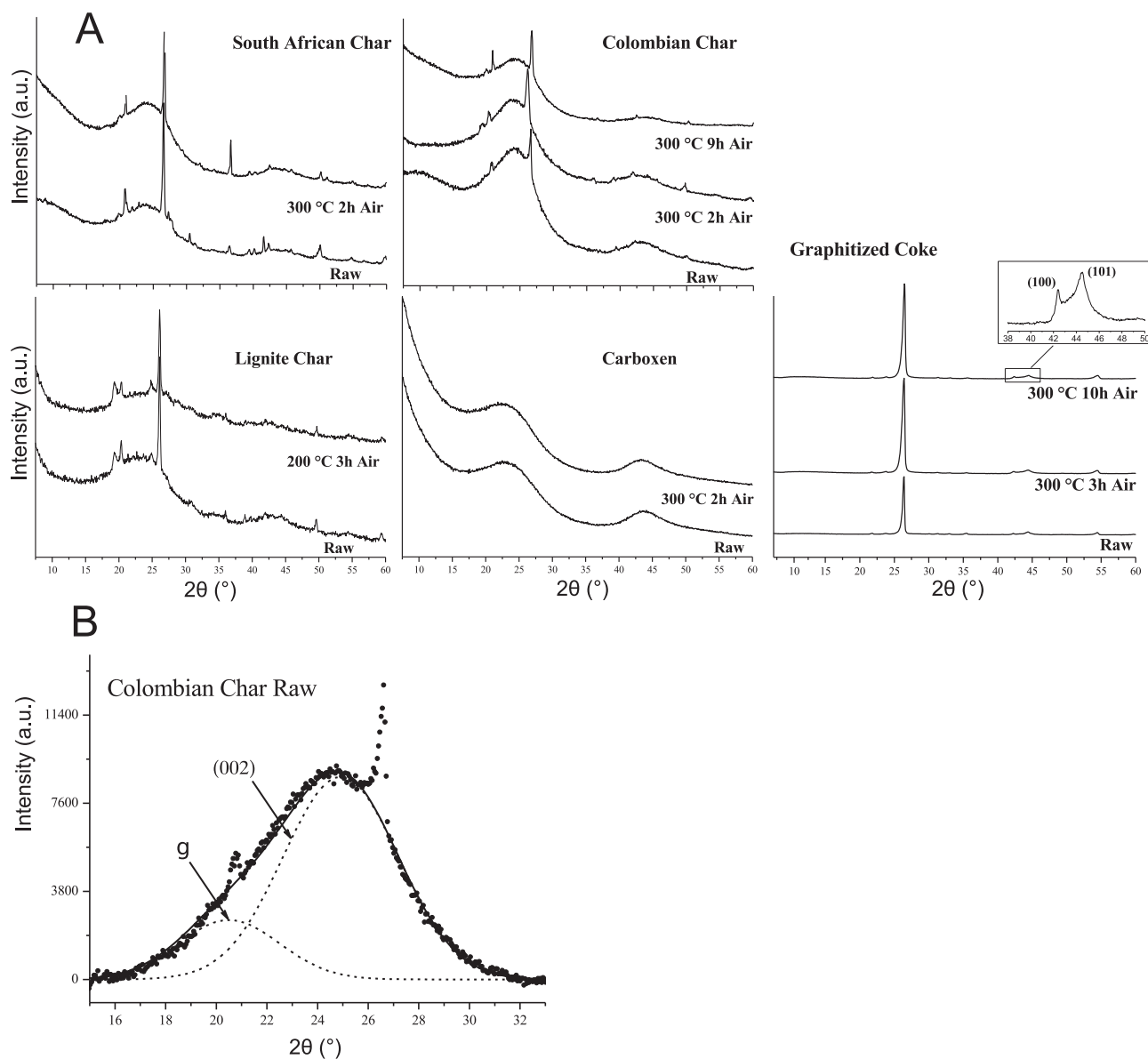
Fig. 4. A. XRD spectra measured on the surface of the samples before and after oxidation. B. Contributions of the (002) and γ bands to the XRD pattern of the raw Colombian coal char after background subtraction and fitting.

coke, however the effects of oxidation on porosity of these samples is quite different: porosity and BET areas are scarcely affected by oxidation at 300 °C in the case of the Carboxen, and are reduced in the case of the South African and Colombian chars. In the case of the Carboxen the modest effects of oxidation can be due to the relatively low combustion reactivity of this sample, which limits the extent of char consumption, combined with the fact that Carboxen is a homogenous material with a readily open microporosity and negligible mineral matter content. For the coal chars, the oxidation conditions are still too mild to induce carbon consumption to an appreciable degree, however oxygen chemisorption can be very relevant, thanks to the presence of meso- and marcopores, which can act as oxygen reservoirs [30], as well as by the presence of mineral matter, which may favour the uptake of oxygen. In fact, in a previous work [31] it was found that at 300°C South African char can gain up to 10 % of weight because of oxygen chemisorption. Oxygen chemisorbed onto the internal area and partially filling the pores would indeed explain the observed reduction of measured BET areas and porosity.

X-ray diffraction analysis

Fig. 4A reports the XRD patterns recorded on the surface of the samples before and after oxidation. The diffractograms of the graphitized coke feature the (002) reflection as a narrow and highly intense peak centred at $2\theta = 26.4°$, and the much less intense (100), (101) and (004) bands at, respectively, 42.3, 44.4 and 54.5° [25-29,32]. Notably, the background intensity is very low, implying a limited presence of amorphous matter as compared to the crystalline fraction. The lack of background intensity from amorphous carbon and the narrowness of the graphitic reflection pattern are related to a high degree of graphitic order.

The turbostratic carbons show high background intensity, which indicates that a significant amount of amorphous carbon is present. The XRD pattern of the turbostratic carbons features the (002) reflection at about $2\theta = 25°$ and the two-dimensional diffraction band at $2\theta \sim 43°$. However, the (002) band is found to be asymmetric. This has been attributed in the literature to superposition of another peak, the γ band, at

Colombian char

Coke

■ 9-10 h   □ 2 h
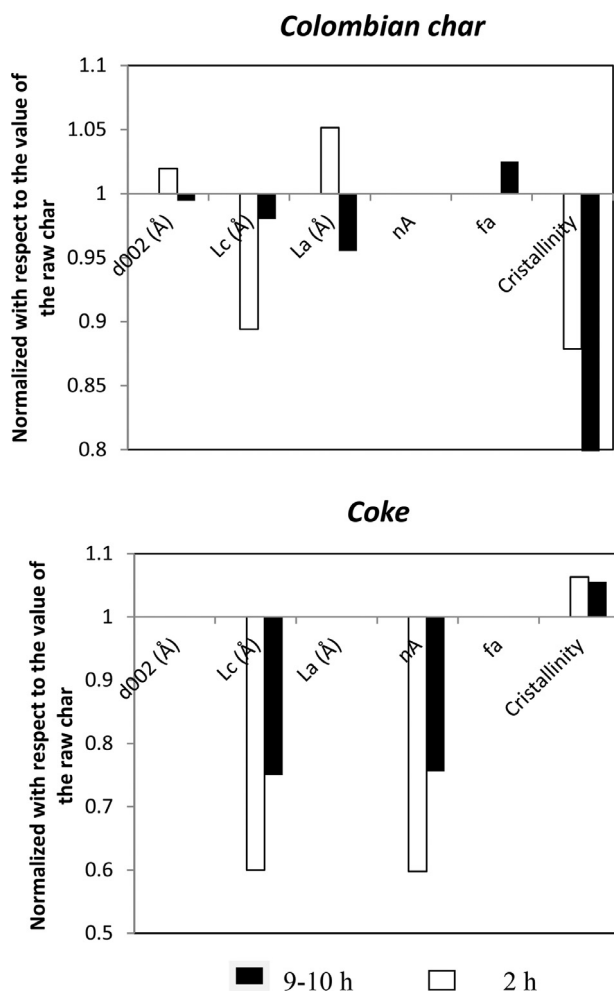
Fig. 5. Ratios between the values of the XRD parameters measured after oxidation at 300°C for different times and before oxidation for the Colombian char (Top) and coke samples (Bottom).

low 2θ values [33,34]. Separation of the contribution of the (002) and γ bands by curve fitting is illustrated in Fig. 4B for the Colombian char sample. The origin of the γ band may be associated with non-aromatic structures, such as aliphatic side chains intercalated between aromatic domains, or randomly oriented crystallites typical of non-graphitized carbon materials. The other peaks in the spectra of the char samples are related to the presence of inorganic matter. In particular, the presence of SiO_2 generates the most intense, narrow reflections at $2\theta \sim 21$ and 26°. No peaks due to inorganic components are present in the spectra of the Carboxen.

The values of the XRD structural parameters for each sample are reported in Table 3.

As expected, the graphitized coke is found to be the only truly crystalline material among all the samples. The average height L_c of the graphitic crystallites is 27 nm and d_{002} is 3.37 Å, the latter being only slightly different from that evaluated on perfect graphitic crystals (3.35 Å) [35]. Due to extensive overlap of the (100) band with the (101) band in the graphitized coke spectra it was not possible to calculate the L_a values for this sample (L_a values for this sample were obtained from the Raman spectra, see next section). These features are an indication of high degree of hexagonal AB stacking. For the raw char samples and the Carboxen the interlayer spacing d_{002} is larger, ranging between 3.50 and 3.68 Å. Such values are typical of random layer lattice or turbostratic carbon structures. L_c increases going from the Carboxen (11.6 Å) to the Colombian char (15.1 Å), correspondingly L_a increases

from 26.9 Å (Colombian char) to 31.9 Å (Carboxen). The average height of the graphite-like crystallites is about half the diameter of the aromatic sheets, which is common for coal-derived materials [5,26,33,36]. Finally, we note that the Carboxen displays crystallites with the smallest thickness and largest diameter.

The values reported in Table 3 reveal that the largest changes in the structural parameters upon mild oxidation are observed for the graphitized coke and the Lignite char, the samples with the highest and lowest degree of graphitic order, respectively. In the case of the coke, oxidation at 300 °C for 2 h results in a decrease of the height of the crystallites and packing (L_c and n_A values), whereas the interlayer distance d_{002} remains relatively unaffected. In the case of the Lignite char, a decrease of the L_c and n_A values is also observed, which is accompanied by a significant decrease in interlayer distance d_{002}. The latter observation can be explained by a partial combustion of this sample, as also indicated by the BET analysis. The ratio of aromatic over aliphatic carbon (f_a) of the Lignite char also decreases, suggesting that for this sample combustion is predominantly consuming aromatic parts. In the turbostratic samples slighter changes are observed upon mild oxidation. The degree of crystallinity increases only in the truly graphitc material, coke, whereas it decreases for all coal chars.

The Colombian char and coke samples were also oxidized at 300°C for more prolonged times (9 and 10 h respectively). The effects of oxidation over longer times can be appreciated in Fig. 5, which reports the ratio of the values measured for the oxidized samples over those of the raw chars. The increase of the L_c and n_A values for the graphitized coke sample after oxidation for 10 h suggests that prolonged oxidation leads to a partial recover of the structural order of the raw material. On the other hand, the crystallinity degree of the Colombian char decreases continuously with oxidation time.

Raman measurements

Fig. 6 reports the Raman spectra measured on the surface of the raw and oxidized samples in the range 950–2200 cm^{-1} after background subtraction and normalization with respect to the G band. The raw graphitized coke exhibits the typical Raman spectrum of polycrystalline graphite, with L_a bigger than 10 nm (see Table 3), featuring a narrow and intense G band at about 1580 cm^{-1} and a broader and much less intense D ('Defect') band at about 1350 cm^{-1}. For the other investigated samples, the D and G bands appear broader and partly overlapping, with maximum intensity at around 1330–1345 cm^{-1} and 1590–1600 cm^{-1}, respectively. Moreover, a broad peak centred at about 1500 cm^{-1} (D3 band), typical of amorphous C sp^2, is observed. The 1150 cm^{-1} band, indicative of sp^2-sp^3 carbon sites, is barely visible in the South African and Colombian chars, and can be appreciated only as a shoulder in the spectra of the Carboxen. Figure 6B illustrates the band decomposition after curve fitting analysis of the Raman spectrum of the raw Colombian char. The full widths at half maximum (FWHM) of the D and G bands, which range from 165 to 224 cm^{-1} and from 61 to 76 cm^{-1}, respectively, and the presence of the D3 band of amorphous carbon are typical of the Raman spectra of turbostratic carbon materials with a low degree of crystalline order and a limited extension of the graphene layers [25]. It can be observed that the FWHM of the D and G bands is significantly higher than for the graphitized coke, denoting a lower degree of graphitization. Furthermore, the additional defective D2 band at ~1620 cm^{-1} had to be included in the fitting of the spectrum for a good enough fit.

The values of the I_D/I_G and I_{D3}/I_G derived from the analysis of the Raman spectra are reported in Table 3 together with the FWHM of the D band. The values of I_D/I_G are indicative of the relative importance of defective over graphitic carbon structure. As expected, this value is the smallest for the sample of coke. The values increase sensibly moving to the turbostratic chars. The value of I_{D3}/I_G, which can be considered an index of the relative amount of sp^2-bonded forms of carbon on the sample surface, is virtually zero for the graphitized coke, due to the

Table 3
Results of XRD and Raman spectroscopy.

Sample	Oxidation	XRD						Raman			
		d_{002} (Å)	L_c (Å)	L_a (Å)	n_A	f_a	Cristallinity %	I_D/I_G	I_{D3}/I_G	$L_a$raman (Å)	FWHM(D) (cm^{-1})
Lignite char	Raw	3.67	13.3	29.6	5	0.77	40.9	2.90	0.40		205
	200 °C 3 h	3.42	11.5	29.5	4	0.70	27.5	3.16	0.48		210
South African char	Raw	3.50	14.5	26.9	5	0.72	66.9	2.62	0.39		204
	300 °C 2 h	3.49	15.1	27.8	5	0.76	63.4	3.01	0.43		205
Colombian char	Raw	3.57	15.1	29.1	5	0.80	64.3	2.74	0.31		194
	300 °C 2 h	3.64	13.5	30.6	5	0.80	56.5	2.51	0.31		215
	300 °C 9 h	3.55	14.8	27.8	5	0.82	49.0	2.79	0.37		224
Carboxen	Raw	3.68	11.6	31.9	4	1.00	49.8	2.82	0.37		165
	300 °C 2 h	3.76	11.8	32.4	4	1.00	49.0	2.77	0.32		170
Graphitized coke	Raw	3.37	272.0		82	1.00	79.3	0.34		128	49.6
	300 °C 3 h	3.37	163.2		49	1.00	84.3	0.41		107	59
	300 °C 10 h	3.37	204.0		62	1.00	83.7	0.08		531	61
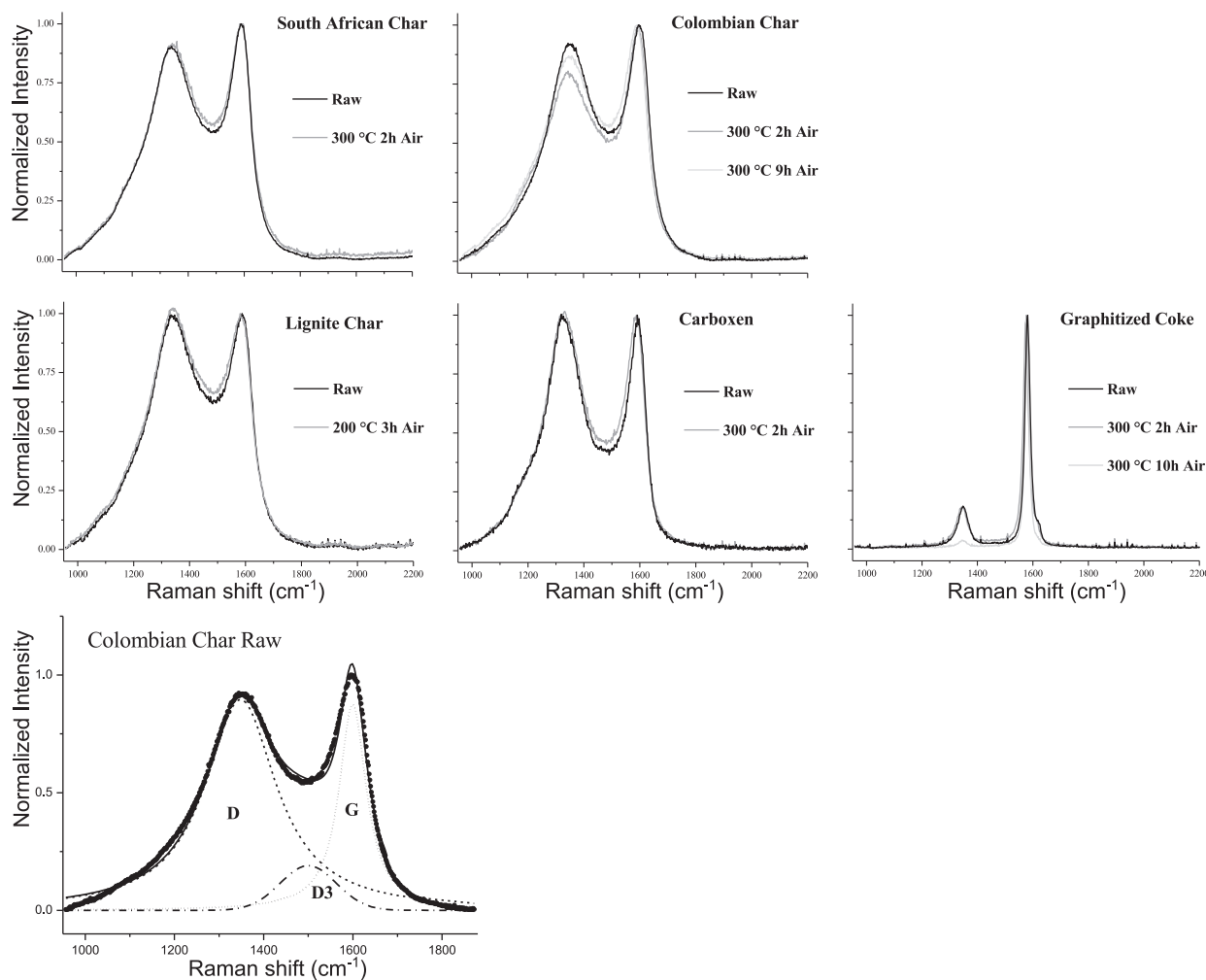
Fig. 6. A. Raman spectra of the samples before and after oxidation. All spectra are normalized with respect to the intensity of the G band. B. Fitting of a Raman spectrum of the Colombian char before oxidation. The dotted and solid lines are relative to the experimental data and the best-fit curves, respectively.

lack of the D3 band, and is maximum in the young and more disordered Lignite char and Carboxen samples. The L_a values have been calculated from Raman only for the graphitized coke and have been reported in Table 3 as $L_a$raman. For the chars the $L_a$raman values are not reported because they are affected by large errors [26].

After oxidation for 2–3 h an increase of the FWHM of the D band occurs, which can be related to a decrease of the mean diameter L_a of the

graphene layers. For the Colombian char the decrease of the I_D/I_G value correlates with the increase of L_a obtained from the XRD measurements. We note that the degree of crystallinity for this sample still decreases as a result of a decrease of the average heights of the graphitic crystallites L_c, as can be seen from Table 3. Extensive oxidation up to 10 h leads to almost complete vanishing of the D band for the graphitized coke, and the L_a value becomes four times larger compared to the raw sample.
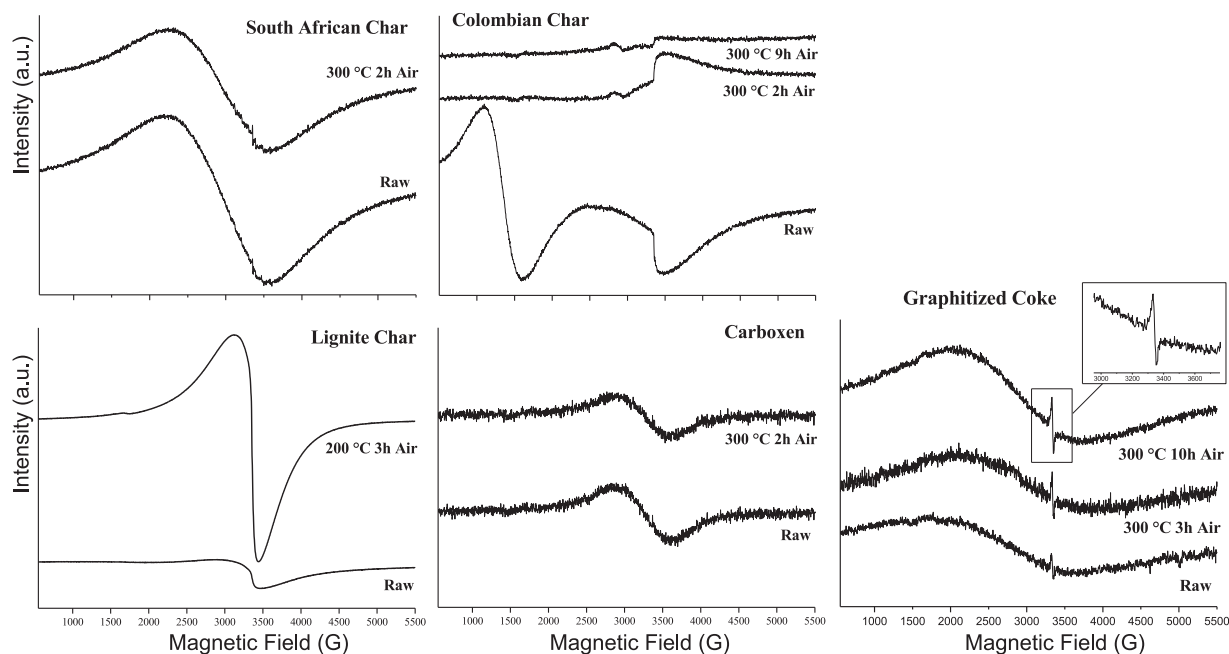
Fig. 7. EPR spectra of the carbon samples before and after mild oxidation.

Table 4
Results of the EPR measurements.

Sample	Oxidation	B (G)	g-band*	$A_{pp}\%$	$\Delta B_{pp}\%$
Lignite char	Raw	3347	1.996 (A)	100	100
	200°C 3h	3357	1.990 (A)	789	55
South African char	Raw	2973	2.247 (A)	100	100
	300 °C 2 h	2979	2.243 (A)	73	100
Colombian char	Raw	3329	2.007 (A)	100	100
		1350	4.949 (P)		
	300 °C 2 h	3336	2.003 (A)	64	66
	300 °C 9 h	3273	2.041 (A)	18	71
Carboxen	Raw	3259	2.050 (A)	100	100
	300 °C 2 h	3264	2.047 (A)	74	98
Graphitized coke	Raw	3336	2.003 (G)	100	100
		2775	2.408 (A)	100	100
	300 °C 3 h	3339	2.001 (G)	182	74
		3001	2.226 (A)	99	98
	300 °C 10 h	3341	2.000 (G)	212	81
		2902	2.302 (A)	174	91

* (A) Amorphous; (G) Graphitic; (P) paramagnetic.

Prolonged oxidation results in an expansion of the graphene layers in the case of the graphitized coke, while no significant changes in the lineshapes of the spectrum of the Colombian char oxidized for 9 h are detected.

Electron paramagnetic measurements

Fig. 7 shows the EPR spectra recorded on the surface of the raw and oxidized samples. The g values, the peak-to-peak amplitudes (A_{pp}) and peak-to-peak widths (ΔB_{pp}) are reported in Table 4. The values of the parameters obtained from the spectra of the oxidized samples were expressed in percentage with respect to the values of the parameters from the spectra of the raw samples. The narrow signal (ΔB_{pp} = 27 G) of the g = 2.003 band of the graphitized coke is characteristic of highly graphitic and poorly activated carbons, whereas the broad peaks (ΔB_{pp} ranging from 584 to 1854 G) present in the spectra of all other samples arise from unpaired electrons on carbonaceous surfaces containing oxy-

gen sites (activated carbon zone). In addition to this, in the spectrum of the raw Colombian char, a very intense peak at g = 4.949 is observed, which can be attributed to paramagnetic centers localized on a metal, possibly high-spin ionic Fe(III) in an oxygen coordination environment [27, 28]. The Carboxen was found to be the sample with the least intense paramagnetic activity, while the Lignite char features the most intense signal.

The evolution of the EPR signals upon oxidation up to 2–3 h varies according to the type of carbon material. In the case of the graphitized coke, oxidation at 300 °C for 3 h induces an increase of A_{pp} and a decrease of the peak-to-peak width of the activated carbon band. As oxidation is prolonged for 10 h, the amplitude of the graphitized carbon band increases. It can be deduced that prolonged oxidation results in the formation of new paramagnetic sites. For the Colombian char oxidation reduces the amplitudes of the band of activated carbon, while producing minor changes in the ΔB_{pp} values. This could be related to a loss of the paramagnetic centers localized on carbon. Furthermore, complete vanishing of the highly polar component (g-band 4.949) in the EPR spectrum occurs after oxidation. As the oxidation time is extended up to 9 h, a further decrease of paramagnetic features with almost complete vanishing of the EPR signal is observed. For the South African char and the Carboxen, oxidation reduces the amplitude of the band of activated carbon. Finally, in the case of the Lignite char, the amplitude of the EPR signal increases upon oxidation by almost an order of magnitude, while the width decreases by nearly 50%.

Discussion

First of all, the measurements performed in the present work provide insights on the structure of the raw carbon materials. The porosimetric analysis shows that the porosity of all the coal chars as well as of the graphitized coke is rather modest. The synthetic char, Carboxen, stems out of the group because, due to its preparation history, it exhibits well-developed meso- and microporosities. The XRD analysis highlights that the only sample with real graphitic order is the graphitic coke. Instead, the coal chars (South African, Colombian and Lignite chars) all exhibit the features typical of turbostratic materials, being characterized by a large contribution of amorphous matter. Fig. 8 shows that a good corre-
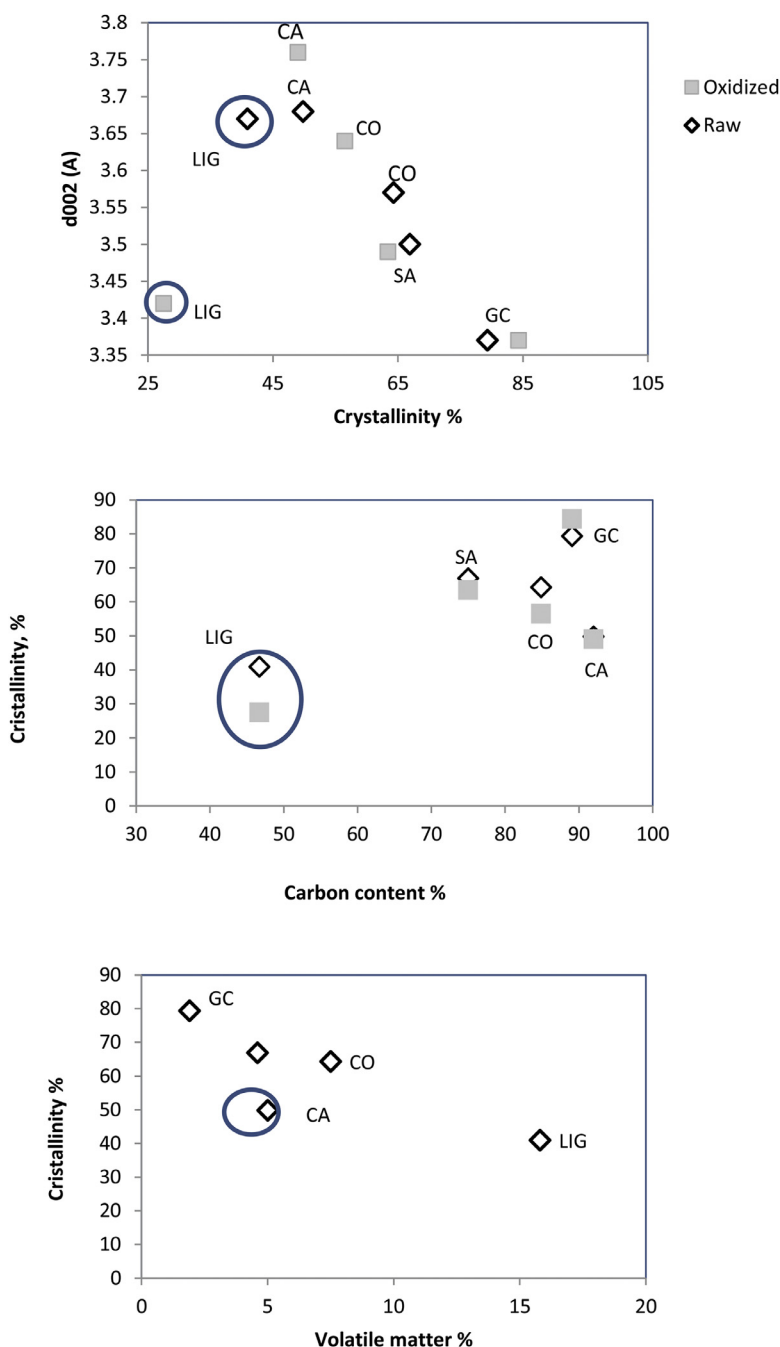
Fig. 8. Correlation between crystallinity and spacing between graphitic layers, carbon content, volatile matter. LIG = Lignite, CA = Carboxen, CO = Colombian, SA = South African, GC = Graphitized Coke.

lation exists between the elemental carbon or volatile matter, which is related to the rank of the coal, and the degree of crystallinity measured by XRD, but again Carboxen stems out of the group with relatively wide and thin crystallites and an overall degree of crystallinity smaller than for a coal char of comparable carbon content. The spacing d_{002} between graphitic layers decreases with increasing degree of crystallinity (see Fig. 8), with the only exception of the Lignite char, which apparently stems out of the group with a distinctively low value of d_{002}.

Raman proved to be less sensitive than XRD in distinguishing differences in the structure of carbon materials of turbostratic characteristics. In fact, differences in Raman features are clearly appreciated only when moving from the graphite to the turbostratic carbons. This finding is consistent with results of a previous study on the effects of thermal an-

nealing on the structure of coal chars [19,37]. In that work chars were produced from given coals using different heat treatments and then analysed by thermogravimetric analysis and Raman to highlight changes in combustion reactivity and structure. It was observed that, while the combustion reactivity of the chars gradually decreased during the heat treatment, thermal annealing did not result in changes of the Raman features up to the most severe heating conditions, when a sharp change in the Raman features occurred.

The experimental analysis also allows to characterize the different responses of the carbon materials to mild oxidation. The porosity of the raw chars is initially quite low. It is known that some degree of combustion can make the internal porosity accessible, but the oxidation conditions adopted in the present work are too mild to result in any carbon
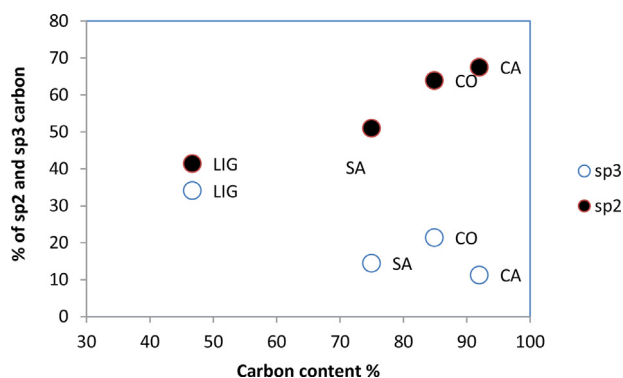
Fig. 9. Correlation between carbon content and % of sp^2 or sp^3 carbon from data reported in [1]. LIG = Lignite, CA = Carboxen, CO = Colombian, SA = South African.

consumption for most of the samples, with the exception of the Lignite char. For this sample, mild oxidation results in an increase of BET area, decrease of aromatic L_c, n_A and d_{002}, decrease of crystallinity and increase of I_D/I_G. These results indicate consumption of carbonaceous matter by combustion, resulting in disruption of the aromatic regions, with possible collapse or compaction of the graphitic islands. In the bituminous Colombian and South African chars, the main result of mild oxidation is to reduce the BET area and the volume of intruded mercury, which may be due to upatake of oxygen with subsequent reduction of the free volume of the pores. XRD and Raman show a slight increase of L_a, f_a and I_D/I_G upon mild oxidation, accompanied by an a decrease of crystallinity degree, and, notably by an increase of d_{002}, which suggests that the formation and rearrangement of C-O complexes causes some slight changes within the carbonaceous structure; in particular the aromatic areas seem to stretch out, but the process is different from graphitization, which would be accompanied also by an increase of crystallinity and other parameters, such as L_c, and n_A. In the graphitic coke upon mild oxidation, even though carbon consumption does not take place due to the low combustion reactivity, several parameters typical of graphitic order (n_A, L_c, L_a) decrease, indicating that the carbonaceous structure is unexpectedly affected. Significantly, the lowest rank carbon material, the Lignite char, and the most graphitic one, the coke, are the samples that undergo the biggest changes upon mild oxidation, even though the effect of the oxidation is different for the two materials. This singularity is further confirmed by the EPR measurements, which show an important activation of carbon upon oxidation only in the case of the Lignite and the graphitized coke. Differently, in the other chars oxidation reduces the EPR signal intensity by quenching the paramagnetic activity of the surface.

The picture emerging from the results of the experimental measurements performed in the present work may benefit from comparison with the results of the XPS experiments presented in a previous article [1] for the same carbon materials. The intensities of sp^2 carbon, sp^3 carbon and of the other carbon functionalites identified in the C1s spectra in reference [1] are plotted in Fig. 9 as a function of the carbon content. It can be observed that for the three coal chars a good correlation exists between C sp^2 content and rank, while the synthetic material, the Carboxen, stems out of the group with a particularly high percentage of sp^2 carbon. In addition, the analysis of the present work shows that Carboxen presents extended micro- and mesoporosities, and relatively wide and thin crystallites. After mild oxidation, a pronounced loss of C sp^2 was observed in all samples by XPS [1], which is confirmed by the Raman results in the present work. XPS clearly demonstrated also a redistribution of the C-O complexes available on the surface upon mild oxidation. In particular, epoxy-type oxygen decreases while ether and carbonyl C-O bonds become predominant. Besides, in the Lignite char, oxidation at 200 °C resulted in formation of new C-O bonds on the surface of the sample. This is confirmed here by the EPR measurements

after oxidation, which show a quenching of the paramagnetic activity in the other coal chars and a pronounced activation of the Lignite. The possibility that some degree of carbon oxidation is occurring in the case of the Lignite char at 200 °C is also suggested by the increase of porosity of this sample

Conclusions

By using different experimental techniques (mercury porosimetry, N_2 adsorption, XRD, Raman spectroscopy, EPR) we have characterized the structure of different carbonaceous materials and assessed the impact of oxidation at mild temperatures on it.

The structural characterization of the raw samples highlights a good correspondence between the rank of the coal and the degree of crystallinity. Alterations of the structural features is significant for the Lignite and the graphitized coke, while the medium rank chars exhibit only slight changes. Porosimetric analysis showed an appreciable increase of porosity upon oxidation for the Lignite char, as a result of partial combustion; otherwise the effect of mild oxidation was to reduce the BET area and the volume of intruded mercury. The EPR activity is seen to increase in the Lignite and coke samples upon oxidation.

These results complement our previous investigation by high-resolution XPS [1] and support the picture that mild oxidation induces the formation of new C-O bonds on the surface of low rank chars, such as Lignite chars, and transformation of already existing C-O species in higher rank coal chars.

Declaration of Competing Interests

The authors declare that they have no known competing financial interests or personal relationships that could have appeared to influence the work reported in this paper.

Acknowledgements

Supplementary materials

Supplementary material associated with this article can be found, in the online version, at doi:10.1016/j.jaecs.2020.100006.

References

[1] Levi G, Senneca O, Causà M, Salatino P, Lacovig P, Lizzit S. Probing the chemical nature of surface oxides during coal char oxidation by high-resolution XPS. Carbon 2015;90:181–96.

[2] Wang H, Dlugogorski B Z, Kennedy E M. Coal oxidation at low temperatures: oxygen consumption, oxidation products, reaction mechanism and kinetic modelling. Prog. Energy Combust. Sci. 2003;29:487–513.

[3] Senneca O, Salatino P, Masi S. The influence of char surface oxidation on thermal annealing and loss of combustion reactivity. Proc Combust Inst 2005;30:2223–30.

[4] Grinberg OY, Williams BB, Ruuge AE, Grinberg SA, Wilcox DE, Swartz HM, Freed JH. Oxygen effects on the EPR signals from wood charcoals: experimental results and the development of a model. J. Phys. Chem. B 2007;111:13316–24.

[5] Knauer M, Carrara M, Rothe D, Niessner R, Ivleva NP. Changes in structure and reactivity of soot during oxidation and gasification by oxygen, studied by micro-Raman spectroscopy and temperature programmed oxidation. Aerosol Sci Technol 2009;43:1–8.

[6] Alonso-Morales N, Gilarranz MA, Heras F, Rodriguez JJ, Eser S. Oxidation reactivity and structure of LDPE-derived solid carbons: a temperature-programmed oxidation study. Energy Fuels 2013;27:1151–61.

[7] Pan R, Tang W, Wu S, Fu D, Jia H. Study on the spontaneous combustion oxidation properties of unloaded coal at various surrounding rock temperatures. Combust Sci Technol 2019.

[8] Pan R-K, Li C, Yu M-G, Xiao Z-J, Fu D. Evolution patterns of coal micro-structure in environments with different temperatures and oxygen conditions. Fuel 2020;261:116425.

[9] Yan Z, Wang D, He R, Teng Y, Liu Q. Microstructural characteristics of Shengli lignite during low-temperature oxidation and promotion effect of iron species. Fuel 2019;255:115830.

[10] Xiao Y, Guo T, Shu C-M, Li QW, Li DJ, Chen LG. Effects of oxygen concentrations on the coal oxidation characteristics and functional groups. J Therm Anal Calorim 2020.

[11] Tang Y, Wang H. Experimental investigation of microstructure evolution and spontaneous combustion properties of secondary lignite. Process Saf Environ Prot 2019;124:143–50.

[12] Li D-J, Xiao Y, Lü H-F, Laiwang B, Shu C-M. Thermokinetic behaviour and functional group variation during spontaneous combustion of raw coal and its preoxidised form. RSC Adv 2020;10(41):24472–82.

[13] Xing B, Zeng H, Huang G, Chen Z, Yu J. Porous graphene prepared from anthracite as high performance anode materials for lithium-ion battery applications. J Alloys Compd 2019;779:202–11.

[14] Shuangyan Cheng, Peiyu Gao, Xiaofan Zang, Yonglong Yang, Hua Bai, Zonghuai Xu, Zhibin Liu. Lei Hierarchically porous carbon by activation of shiitake mushroom for capacitive energy storage. Carbon 2015;93:315–24.

[15] Jiang C, Ma J, Corre G, Jain SL, Irvine JTS. Challenges in developing direct carbon fuel. Cells Chem Soc Rev 2017;46(10):2889–912.

[16] Cao Tianyu, Huang Kevin, Shi Yixiang, Cai Ningsheng. Recent advances in high-temperature carbon–air fuel cells. Energy Environ. Sci. 2017;10:460–90.

[17] Lu Y, Zhao C, Qi X, Qi Y, Li H, Huang X, Chen L, Hu Y-S. Pre-oxidation-tuned microstructures of carbon anodes derived from pitch for enhancing Na storage performance. Adv Energy Mater 2018;8(27).

[18] Levi G, Causà M, Lacovig P, Salatino P, Senneca O. Mechanism and thermochemistry of coal char oxidation and desorption of surface oxides. Energy Fuels 2017;31(3):2308–16.

[19] Bar-Ziv E, Zaida A, Salatino P, Senneca O. Diagnostics of carbon gasification by raman microprobe spectroscopy'. Proc Combust Inst 2000;28:2369–74.

[20] Lu L, Sahajwalla V, Konga C, Harris D. Quantitative X-ray diffraction analysis and its application to various coals. Carbon 2001;39 1821–1833.

[21] Yen TF, Erdman JG, Pollack SS. Investigation of the Structure of Petroleum Asphaltenes by X-Ray Diffraction. Anal. Chem. 1961;33:1587–94.

[22] Van Doorn J, Vuurman MA, Tromp PJJ, Stufkens DJ, Moulijn JA. Correlation between raman spectroscopic data and the temperature-programmed oxidation reactivity of coals and carbons. Fuel Process Technol 1990;24:407–13.

[23] Marquardt DW. An algorithm for least-squares estimation of nonlinear parameters. J Soc Indus Appl Math 1963;11:431–41.

[24] Fujimoto H. Theoretical X-ray scattering intensity of carbons with turbostratic stacking and AB stacking structures. Carbon 2003;41:1585–92.

[25] Tunistra F, Koenig JL. Raman spectrum of graphite. J. Chem. Phys 1970;53:1126–30.

[26] Ferrari AC, Robertson J. Interpretation of Raman spectra of disordered and amorphous carbon. Phys Rev 2000;B61:14095–107.

[27] Ottaviani MF, Mazzeo R. EPR characterization of graphitized and activated micro- and meso-porouscarbons. Microporous Mesoporous Mater 2011;141:61–8.

[28] Ottaviani MF, Retini G, Cangiotti M, Mangani F, Segre U. Characterization of the surface interacting ability of carbon black by means of electron paramagnetic resonance analysis of adsorbed Cu2+, supported by surface analysis and atomic absorption. Spectrochimica Acta A 2002;58:1129–41.

[29] Gregg SJ, Sing KSW. Adsorption, surface area & porosity. Academic, London, 2nd edition; 1982.

[30] Salatino P, Senneca O, Masi S. Gasification of a coal char by oxygen and carbon dioxide. Carbon 1998;36:443.

[31] Senneca O, Salatino P. Assessment of the thermochemistry of oxygen chemisorption and surface oxide desorption during looping combustion of coal char. Proc Combust Inst 2013;34(2):2787–93.

[32] Cuesta A, Dhamelincourt P, Laureyns J, Martínez-Alonso A, Tascón JMD. Comparative performance of X-ray diffraction and Raman microprobe techniques for the study of carbon materials. J. Mater. Chem 1998;8:2875–9.

[33] Lu L, Sahajwalla V, Konga C, Harris D. Quantitative X-ray diffraction analysis and its application to various coals. Carbon 2001;39 1821–1833.

[34] Yen TF, Erdman JG, Pollack SS. Investigation of the structure of petroleum asphaltenes by X-ray diffraction. Anal. Chem. 1961;33:1587–94.

[35] Baskin V, Meyer L. Lattice constants of graphite at low temperatures. Phys Rev 1955;100:544.

[36] Mapelli C, Castiglioni C, Meroni E, Zerbi G. Graphite and graphitic compounds: vibrational spectra from oligomers to real materials. J Mol Struct 1999:480–1.

[37] Livneh T, Bar-Ziv E, Senneca O, Salatino P. Evolution of reactivity of highly porous chars from Raman microprobe spectrometry. Combust. Sci. and Tech 2000;153:65.